Elastic Polarizable Environment Cluster Embedding Approach for Covalent Oxides and Zeolites Based on a Density Functional Method

Vladimir A. Nasluzov,*,† Elena A. Ivanova,† Alexei M. Shor,† Georgi N. Vayssilov,*,‡ Uwe Birkenheuer,§,∥ and Notker Rösch*,§

Institute of Chemistry and Chemical Technology, Russian Academy of Sciences, 660049 Krasnoyarsk, Russia, Faculty of Chemistry, University of Sofia, 1126 Sofia, Bulgaria, and Institut für Physikalische und Theoretische Chemie, Technische Universität München, 85747 Garching, Germany

Received: August 12, 2002; In Final Form: January 10, 2003

We present a new quantum mechanics/molecular mechanics (QM/MM) embedding approach for systems with directional polar covalent bonds. This "covalent elastic polarizable environment" (covEPE) scheme features a variational treatment of an energy expression that includes all degrees of freedom of both the QM region (the "cluster") and the MM regions (the "environment"). The method completely and explicitly includes both the electrostatic and mechanical interactions between a QM model cluster and its environment. Monovalent pseudoatoms that represent real atoms of the material saturate the dangling bonds of the cluster; these pseudoatoms belong simultaneously to the QM and MM regions. For a correct description of a pure silica environment, we constructed a new force field of the shell-model type based on potential derived charges instead of formal charges. We implemented the covEPE approach in the density functional program ParaGauss and applied it to pure-silica and Al-containing chabazite, employing a generalized gradient approximation. These applications showed that calculated structural parameters and OH frequencies of bridging hydroxyl groups reproduce experimental data with good accuracy compared to other contemporary computational methods.

1. Introduction

Currently, there is a high demand for realistic, yet feasible computational modeling of oxides and zeolites. In response, various quantum mechanical/molecular mechanics (QM/MM) computational schemes were developed, combining a QM treatment of an active site with a classical MM modeling of its environment.[1−4] These "hybrid" or embedding QM/MM methods allow one to account for major effects of the surrounding framework on the properties of the active site, in particular for effects due to specific steric restrictions and the long-range electrostatic potential. Such accurate modeling is not possible with an isolated cluster approach.[5]

Substantial complications in QM/MM schemes for covalent oxides and zeolites arise from the necessity to cut a QM cluster from a covalent framework of the surrounding material. Consequently, unsaturated covalent bonds appear for atoms at the boundary of the QM cluster. In most embedding methods reported, these "dangling" bonds are terminated by H atoms, referred to as link atoms, with special restrictions for the length and orientation of the saturating bond.[1−4] Because these link atoms are not present in the real system, one attempts to eliminate their contribution to the energy of the system by a subtraction scheme of the type suggested by Morokuma et al.[6] for organic compounds and complexes. However, a precise (complete) subtraction can be achieved only when the inter-

atomic potentials used in the MM calculation are fitted to reproduce structure and energy variations related to deformations at the cluster border calculated at the QM level. Sauer and co-workers established such a strategy at the Hartree−Fock (HF) and density functional (DF) levels of their QM-Pot (QM-potential) scheme;[1] this approach correctly represents steric constraints of the framework. However, the polarization of the electron density of the QM cluster by the Coulomb field of the environment is not taken into account. Actually, this is a general deficiency of all QM/MM methods based on the "subtraction" strategy, because the QM calculations of the cluster are completely separated from the MM calculations; i.e., the charge distribution of the environment does not affect the QM cluster. Sherwood et al.[2] attempted to overcome this deficiency of the subtraction scheme;[2] similarly to the approach described by Thiel and co-workers,[7] they used both mechanical and electrostatic coupling between the QM and MM systems without subtracting the contribution of the link atoms from the energy of the system. In this method, the electrostatic potential of the MM region contributes to the electronic Hamiltonian of the cluster and the polarization of the classical region due to variations of the charge density in the QM cluster is accounted for. However, the presence of link atoms in artificial positions of the structure of the framework (too close to some of the "real" atoms) required a special rearrangement of the charges on atoms of the MM part, which are close to link atoms.[2] As a result, the electrostatic potential near the border between QM and MM regions is strongly perturbed and likely influences both the QM cluster and the guest species in an undesirable fashion.

Yet another type of embedding scheme focuses only on long-range electrostatic effects of the surrounding framework on the QM cluster; mechanical interactions are not included.[3] The

*　* Authors to whom correspondence should be addressed. E-mail: nv@krsk.infotel.ru, gnv@chem.uni-sofia.bg, and roesch@ch.tum.de.
　† Russian Academy of Sciences.
　‡ University of Sofia.
　§ Technische Universität München.
　∥ Present address: Max-Planck-Institut für Physik komplexer Systeme, 01187 Dresden, Germany.*

electrostatic potential of the environment is included in the Hamiltonian of the QM cluster either via an array of point charges (PC) located at crystallographic positions or as a correction potential derived from periodic calculations on the unperturbed structure of the environment. However, both strategies require special rearrangements of the charges at the border region due to the presence of bond-capping H atoms at the QM cluster.[3] In addition, the structural relaxation of the cluster is not approximated properly, because the mechanical coupling is neglected.

The goal of the present work is a new QM/MM cluster embedding approach that is suitable for covalent oxides and zeolites; this new embedding scheme combines both mechanical and electrostatic interactions between the QM and MM parts of the system and overcomes deficiencies of other methods connected with the presence of artificial H link atoms between the two regions. Our approach is a modification of the elastic polarizable environment (EPE) embedding procedure for ionic oxides that we presented recently for fully ionic materials.[8] We demonstrated the power of the approach for metal adsorption on MgO(001)[8] and CO adsorption at α-Al$_2$O$_3$.[9]

Here, we will extend this scheme to describe a "covalent elastic polarizable environment" (covEPE) for (ionic) systems with directional polar covalent bonds. In the EPE approach to ionic as well as polar covalent systems, the QM cluster is terminated with pseudopotential capping atoms. Whereas capping atoms of ionic oxides are represented by effective core potentials without basis functions,[8] the QM cluster in the covEPE scheme is saturated by specially constructed monovalent "pseudoatoms", referred to as bonding atoms. Note that these bonding atoms represent real atoms of the material which simultaneously belong to both QM and MM regions. Pseudoatoms are constructed in analogy to the pseudobond embedding approach.[10] To represent the electronic and geometry structure of the border region properly, pseudopotential parameters have to be optimized to reproduce the characteristics of an analogous cluster treated with the QM method. In the current covEPE implementation, such bond capping border centers are located at anionic positions of oxygen atoms of the silicate framework.

This covEPE QM/MM scheme overcomes several drawbacks of previous embedding schemes: (i) it completely and explicitly includes both electrostatic and mechanical interactions of a cluster and its surrounding, (ii) it avoids complications connected with the use of hydrogen link atoms at the QM cluster border, and (iii) like the EPE method for polar oxides,[8] it features a variational treatment of an energy expression that includes all degrees of freedom of both QM and MM regions. Furthermore, calculations in the present QM/MM scheme account for the polarization of the environment by the QM cluster, a feature lacking in most popular QM/MM schemes for describing systems with covalent Si−O bonds. Very recently, a similar embedding scheme was proposed for silica.[11] Both schemes are variational and treat active centers in a crystal as point defects of the periodic structure. There are two main differences between the approach of Sulimov et al.[11] and the present covEPE scheme: (i) they choose Si atoms as border centers and add a special sp orbital, whereas we choose O atoms as border atoms; (ii) the covEPE approach offers an internally consistent treatment based on values of point charges of the environmental centers chosen to reproduce, at a distance, the electrostatic potential of the corresponding fragment of crystal when described quantum chemically. To achieve such a consistent treatment, we generated a special force field parametrization for the environment that satisfies all requirements for such a purpose; on the other hand,
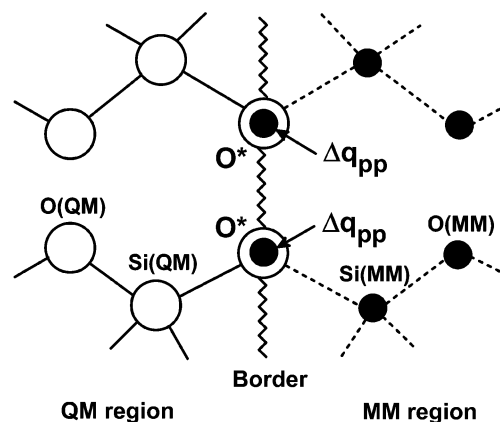

Figure 1. Construction of the border region between a QM cluster and its MM environment. The atoms participating in the QM part are shown as open circles, and the centers of the MM part are shown as filled circles. Solid and dashed lines denote bonding between atoms in the QM cluster and the MM part, respectively.

the ionic charges used in ref 11 are rather large (two times larger than the potential derived charges (PDC) employed in our calculations). With our new PDC-based shell model force field, we aimed, in particular, at an accurate representation of the electrostatic potential of the surrounding.

In section 2, we will describe the covEPE embedding scheme. Details of the implementation and the parametrization are discussed in section 3. In section 4, we will present an application of the covEPE method to pure-silica and Al-containing chabazite.

2. Description of covEPE Embedding Scheme

2.1. Partitioning of the System. We partition our system into two main parts: quantum region I (QM cluster) and region II treated classically, also referred to as elastic polarizable environment (EPE lattice). The QM cluster comprises that part of the framework of the material containing the active site (bridging OH group, metal cation, basic oxygen centers, etc.) and its immediate neighboring atoms. All adsorbate molecules or guest species interacting with the active site are also considered to be part of the QM region. As discussed in the Introduction, one of the most complicated problems of various hybrid QM/MM schemes is the construction of the border region between the QM and the classical regions where covalent bonds are cut. We tried to overcome such complications by locating the border at real atoms of the system (Figure 1). Our approach has the advantage that it does not introduce artificial link atoms. Border atoms belong simultaneously to the QM and the classical regions; they interact classically with the lattice, and they contribute as pseudopotential atoms to the Hamiltonian of the embedded QM cluster (Figure 1). As part of the QM cluster, the border atoms of the covEPE approach are represented by monovalent seven-electron pseudoatoms featuring an orbital basis set and a specially adapted pseudopotential. As part of the classical lattice, border atoms are considered as lattice centers with a modified charge. We choose to cut the system along oxygen centers, because they are present in all covalent oxides, zeolites, and other molecular sieve structures; thus, we are able to use the same scheme of embedding with oxygen-terminated clusters in simulations of all these structures. To achieve the optimal description of the border region, the pseudopotential of border oxygen centers O* has to be adjusted for each set of terminal pseudobonds, i.e., for each set of neighboring atoms on either side, the lattice, and the QM region.[12]

To reproduce the polarization of the environment, the centers in region II (EPE) are treated in a shell model approach.[13] Cationic centers (e.g., Si, Al, Ti) are considered as point charges, and polarizable anions (O) are represented by two (formal) point charges (PC): q_{core} for the core, and q_{shell} for the shell (with different coordinates). The total charge of an anion is $q_{tot} = q_{core} + q_{shell}$. The two PCs representing an anion interact via a harmonic pair potential with a force constant that allows reproduction of the polarizability of the ion. We choose the charges q_{lat} of all lattice centers as PDC,[14] such that they reproduce the electrostatic potential of the corresponding lattice as it is obtained from high-level electronic structure calculations. In this way, the long-range interaction of the lattice ions with the QM cluster (which is a part of the framework) and any adsorbate will be adequately described. For convenience, we will consider core and shell charges as part of the set of all centers of the lattice, the coordinates of which will be collectively referred to as R_{lat}. In addition to electrostatic interactions, the cationic centers and the shells of polarizable ions of the lattice participate in "short-range" interactions that represent covalent interactions (including Pauli repulsion) with neighboring lattice centers.

Since the border atoms O* represent the internal border of the classical lattice, they are bonded to only one cationic center of the lattice (Si or another center), whereas normal oxygen centers inside the lattice are bonded to two cationic centers. To properly balance the charge distribution of the whole system, one may consider the charge of each center in region II to result from incremental contributions due to each bond in which the corresponding center participates. By this argument, the incremental charge Δq_{pp} of a border center O* as part of the molecular mechanical lattice should be half the charge of an oxygen center inside the lattice. The total charge of a border center O* is the sum of the charge increments Δq_{pp}, of the nuclear charge, and of the effective electronic charge. The polarization of O* is described only on the QM level, no core–shell splitting is considered.

2.2. Energy. The total energy (E_{tot}) of the system under consideration is the sum of the energies of both parts, cluster and lattice (E_{cl} and E_{lat}) and their interaction E_{int}

$$E_{tot} = E_{cl}^{QM}(\rho_{cl}^{QM}, R_{cl}, R_{pp}) + E_{lat}^{MM}(\rho_{lat}, R_{lat}, R_{pp}) + E_{int}(\rho_{cl}^{tot}, R_{cl}, R_{pp}, \rho_{lat}, R_{lat}) \quad (1)$$

The first term (E_{cl}^{QM}) represents the energy of interactions acting only within the cluster described by the QM method. This energy depends on the positions (R_{cl}) of the atoms inside the cluster, on the positions (R_{pp}) of the border atoms O*, and on the electron density distribution (ρ_{cl}^{QM}) of the QM cluster.

The energy (E_{lat}^{MM}) of the lattice is calculated with an appropriate force field (FF) that accounts for the interactions between the atoms in region II, also including their interactions with border atoms O*. This lattice energy comprises (i) the Coulomb interaction (V_{Coul}); (ii) short-range interactions (V_{short})-including interatomic repulsion, dispersion interactions, and three-body interactions (valence angle); and (iii) the core–shell interaction ($V_{core-shell}$) at each polarizable center of the lattice. The energy (E_{lat}^{MM}) depends on the positions (R_{lat}) of the atoms inside the lattice (core and shell centers are considered separately) and the positions (R_{pp}) of the border atoms.

The coupling term E_{int} contains two contributions.

The first contribution is the long-range electrostatic interaction between the total charge density ($\rho_{cl}^{tot,QM}$) of the QM cluster and the total charge density of the lattice, ρ_{lat}. The former comprises the electron charge density (ρ_{cl}^{QM}), the nuclear charges ($q_{cl}^{N}(R_{cl})$) of atoms inside the cluster, and the nuclear charges ($q_{pp}^{N}(R_{pp})$) of border atoms; the latter includes the charges ($q_{lat}(R_{lat})$) of all ions, cores, and shells of the lattice at the corresponding positions as well as the charges on the atoms O*. Note that the interaction of ρ_{cl}^{QM} with the external electrostatic potential is accounted for through the matrix elements calculated with the basis functions (see section 3.3) and that the interaction between nuclear charge and point charge of a given border atom O* is excluded.

The second contribution is the short-range nonbonding host–guest interaction between the atoms inside the QM cluster and guest species as part of the QM cluster (when present) and centers of the MM region.

Thus, the total energy of the system can be written as

$$E_{tot} = E_{cl}^{QM}(\rho_{cl}^{QM}, q_{cl}^{N}(R_{cl}), q_{pp}^{N}(R_{pp})) + V_{Coul}(q_{lat}, \Delta q_{pp}, R_{lat}, R_{pp}) + V_{short}(R_{lat}, R_{pp}) + V_{core-shell}(R_{lat}) + [\rho_{cl}^{tot,QM}(\rho_{cl}^{QM}, q_{cl}^{N}(R_{cl}), q_{pp}^{N}(R_{pp}))||\rho_{lat}(q_{lat}(R_{lat}), \Delta q_{pp}(R_{pp}))] + V_{short}(R_{cl}/R_{lat}) \quad (2)$$

The notation $[\rho_1||\rho_2]$ designates the Coulomb interaction between two charge distributions, ρ_1 and ρ_2. The term $V(R_m, R_n)$ denotes the potential energy due to interactions among all atoms of the sets in question (with coordinates R_m and R_n, respectively), including the interactions within each set; by the notation $V(R_m/R_n)$, we refer to the interactions between atoms of one set, R_m, with atoms of another set, R_n. For computational convenience, we consider the charge increments (Δq_{pp}) of O* border atoms as a correction to the nuclear charge of the corresponding border atom, namely

$$q_{pp}^{N*} = q_{pp}^{N} + \Delta q_{pp} \quad (3)$$

With this modification, we obtain the following forms of the three energy expressions:

$$E_{cl}^{QM} = E_{cl}^{QM}(\rho_{cl}^{QM}, q_{cl}^{N}(R_{cl}), q_{pp}^{N*}(R_{pp})) \quad (4)$$

$$E_{lat}^{MM} = V_{Coul}(q_{lat}, R_{lat}) + V_{short}(R_{lat}) + V_{core-shell}(R_{lat}) \quad (5)$$

$$E_{int} = [\rho_{cl}^{tot,QM}(\rho_{cl}^{QM}, q_{cl}^{N}(R_{cl}), q_{pp}^{N*}(R_{pp}))||\rho_{lat}(q_{lat}(R_{lat}))]$$
$$+ V_{short}(R_{cl}, R_{pp}/R_{lat}) \quad (6)$$

The terms for the short-range interactions of O* border atoms with lattice centers are now included in E_{int}, because this term accounts for the interactions between the two subsystems.

2.3. Strategy for Self-Consistent Treatment. Due to the different computational treatment of regions I and II by QM and MM methods, respectively, we have to expect an artificial distortion of the structure of the embedded system compared to a system treated completely classically, even without any guest species, impurities, or defects. To eliminate this artificial distortion, we follow the strategy recently developed for the ionic version of the EPE method.[8] This approach is based on two preliminary optimization steps for the ideal system:

Step 1 comprises a classical treatment of the whole unperturbed (regular) system with the same FF chosen for the MM modeling of the environment. The equilibrium geometry of the system is produced by minimizing the total energy (E_{tot}^{MM}) which depends on the coordinates of ions, core, and shell charges. The resulting equilibrium values of all coordinates, of

Covalent Oxides and Zeolites

J. Phys. Chem. B, Vol. 107, No. 10, 2003 **2231**

both cluster and lattice, of the regular structure are denoted by the superscript reg (R_{cl}^{reg}, R_{pp}^{reg}, R_{lat}^{reg}). The corresponding charge distribution of the cluster obtained in this step is denoted as $\rho_{cl}^{tot,MM}(R_{cl}^{reg}, R_{pp}^{reg})$, where the coordinates of the shells of polarizable centers in the cluster (region I) are also included.

Step 2 provides a reference calculation of the cluster, treated quantum mechanically, embedded in the regular (unperturbed) environment, as represented by the frozen lattice with the configuration obtained in step 1. One minimizes E_{tot} with respect to the electron distribution of the cluster, the coordinates of the atoms inside the QM cluster, and the border atoms for fixed values of $R_{lat} = R_{lat}^{reg}$. The resulting equilibrium values of the coordinates are R_{cl}^{ref} and R_{pp}^{ref}, and the corresponding charge distribution is $\rho_{cl}^{tot,QM}(\rho_{cl}^{ref,QM}, R_{cl}^{ref}, R_{pp}^{ref})$.

Both charge densities, $\rho_{cl}^{tot,MM}(R_{cl}^{reg}, R_{pp}^{reg})$ and $\rho_{cl}^{tot,QM}(\rho_{cl}^{ref,QM}, R_{cl}^{ref}, R_{pp}^{ref})$ obtained in steps 1 and 2, respectively, represent the unperturbed cluster and thus, ideally, should coincide. To approach this requirement, we fix the charge distribution of the unperturbed QM cluster, treated with the full covEPE embedding procedure, at $\rho_{cl}^{tot,MM}(R_{cl}^{reg}, R_{pp}^{reg})$ as obtained in step 1 for the complete regular system. Also, we replace the charge density distribution $\rho_{cl}^{tot,QM}(\rho_{cl}^{QM}, R_{cl}, R_{pp})$ of the cluster obtained in the QM calculation by an effective charge distribution

$$\rho_{cl}^{tot,eff}(\rho_{cl}, R_{cl}, R_{pp}) = \rho_{cl}^{tot,QM}(\rho_{cl}^{QM}, R_{cl}, R_{pp}) - \rho_{cl}^{tot,QM}(\rho_{cl}^{ref,QM}, R_{cl}^{ref}, R_{pp}^{ref}) + \rho_{cl}^{tot,MM}(R_{cl}^{reg}, R_{pp}^{reg}) \quad (7)$$

This effective charge density is used in all covEPE calculations (see below). Contributions pertaining to a guest species (adsorbate) are included neither in the (cluster) reference charge density ($\rho_{cl}^{ref,QM}$) nor in the regular charge density ($\rho_{cl}^{tot,MM}$) of the cluster; they appear only in the charge density $\rho_{cl}^{tot,QM}(\rho_{cl}^{QM}, R_{cl}, R_{pp})$, obtained in the QM calculation of the embedded cluster. Note that R_{cl} in steps 1 and 2 and R_{cl} for the complete EPE system (first term on the right-hand side of eq 7) differ by the coordinates of a guest species (if present).

In a similar way, we correct the short-range interaction potential ($V_{short}(R_{cl}, R_{pp}/R_{lat})$) as follows:

$$V_{short}^{eff}(R_{cl}, R_{pp}/R_{lat}) = V_{short}(R_{cl}, R_{pp}/R_{lat}) - V_{short}(R_{cl}^{ref}, R_{pp}^{ref}/R_{lat}^{ref}) + V_{short}(R_{cl}^{reg}, R_{pp}^{reg}/R_{lat}^{reg}) \quad (8)$$

Again, coordinates of guest species are included in the first term, $V_{short}(R_{cl}, R_{pp}/R_{lat})$, but missing in the two remaining terms. This potential correction prevents artificial alterations of short-range interactions between cluster and lattice when the cluster is treated at the QM instead of the classical level.

Using these effective quantities, we construct an effective interaction energy expression:

$$E_{int}^{eff} = [\rho_{cl}^{tot,eff}(\rho_{cl}, R_{cl}, R_{pp})||\rho_{lat}(R_{lat})] + V_{short}^{eff}(R_{cl}, R_{pp}/R_{lat}) \quad (9)$$

This expression can be separated into two parts: the interaction energy calculated without corrections of charge distribution and short-range interaction, E_{int} (eq 6), and the correction terms, E_{int}^{corr}

$$E_{int}^{corr} = [(\rho_{cl}^{tot,MM}(R_{cl}^{reg}, R_{pp}^{reg}) - \rho_{cl}^{tot,QM}(\rho_{cl}^{ref}, R_{cl}^{ref}, R_{pp}^{ref}))||\rho_{lat}(R_{lat})] + V_{short}(R_{cl}^{reg}, R_{pp}^{reg}/R_{lat}) - V_{short}(R_{cl}^{ref}, R_{pp}^{ref}/R_{lat}) \quad (10)$$

The correction term E_{int}^{corr} depends on the results of the preparatory steps 1 and 2 but affects only lattice atoms (i.e., for a given lattice configuration, it does not influence the QM

self-consistency cycle). Now we construct the total EPE energy of the system (see eq 6)

$$E_{tot}^{EPE} = E_{cl}^{QM} + E_{lat}^{MM} + E_{int}^{eff}$$
$$= E_{cl}^{QM} + E_{int} + E_{lat}^{MM} + E_{int}^{corr} \quad (11)$$

The last two terms of the last equation affect only the lattice; hence, they constitute an effective energy of the lattice

$$E_{lat}^{eff} = E_{lat}^{MM} + E_{int}^{corr} \quad (12)$$

which includes all corrections that are necessary to maintain the structure of the system in the absence of guest species or defects to that of the regular system.

This construction of the total EPE energy of the system allows us to carry out a complete variational treatment of total energy that includes all degrees of freedom of both QM and MM regions.

3. Implementation of the covEPE Method

We implemented the covEPE embedding scheme in the density functional program ParaGauss for parallel computers.[15,16] First applications will address the structure of pure-silica and H-chabazite as well as the OH vibrational frequency and deprotonation energies of the latter material. In the following section, we describe details of the implementation and the selection of pertinent parameters, including a new FF parametrization for silicates.

3.1. Density Functional Calculations of the QM Region. All applications were carried out with the linear combination of Gaussian-type orbitals fitting functions density functional method (LCGTO-FF-DF)[17] as implemented in the PARAGAUSS program.[15,16] We used the gradient-corrected exchange-correlation functional suggested by Becke (exchange) and Perdew (correlation).[18] The Kohn−Sham orbitals were represented by Gaussian-type basis sets: (6s1p) → (4s1p) for H, (9s5p1d) → (5s4p1d) for O and C, (12s9p2d) → (6s4p2d) for Al and Si.[19] All contractions were of generalized form. For calculating the Hartree contribution of the electron−electron interaction, an auxiliary basis set was employed to represent the electronic charge density.[17] The exponents of the auxiliary basis set were constructed by scaling the exponents of the orbital basis;[17] a standard set of p and d polarization exponents was added on each atomic center.[20] The exchange-correlation energy and the matrix elements of the exchange-correlation potential were evaluated by an accurate numerical integration.[21,22] The structure of the system was optimized using analytical energy gradients[23] and the Broyden−Fletcher−Goldfarb−Shanno Hessian update scheme.[24]

After geometry optimization of H-chabazite model clusters, the vibrational frequency of the bridging OH group was evaluated in the approximation of one independent harmonic oscillator. This assumes a rigid connection between the OH group under study and the rest of the cluster, while infinitely large force constants are assigned to other internal oscillators of the cluster. This choice is justified by the strong bond between the hydroxyl and the zeolite framework.[25] The force constant of such an approximate vibrational mode was obtained numerically by finite differences of analytical energy gradients.

3.2. Force Field with Potential Derived Charges. As mentioned in the Introduction and in section 2.1, our covEPE implementation requires a FF (for a silicate environment) that relies on the shell model for describing the polarizability of the
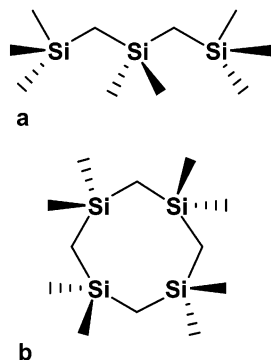
Figure 2. Clusters used for estimating potential-derived charges: (a) 3T linear chain, (b) 4T four-ring.

anions and is based on PDC charges of all lattice centers. Both features are necessary to properly represent the electrostatic interaction between the lattice and the QM cluster. Surprisingly, we were not able to locate a suitable FF in the literature. Common shell model force fields[1b,29] are based on formal charges that would result in an unrealistic Madelung field acting on the covEPE embedded QM cluster. On the other hand, reported force fields adjusted to PDC describe anions by simple point charges only.[30] Combining parameters from different force fields violates the consistency of a FF, and hence, it is not feasible. Furthermore, for an adequate mechanical coupling of a QM cluster and the MM environment, the cluster has to match the size of the corresponding lattice cavity very well. To achieve this goal, it is advisable to use the same quantum mechanical method, namely, Becke−Perdew (BP) DF calculations, for both the QM cluster treatment and the derivation of the FF parameters. For these reasons, we decided to construct a new FF, suitable for our needs. In the following section, we describe the choice of the potential derived charges and the optimization of force field parameter for silica, the environment chosen in subsequent applications (section 4).

3.2.1. Charges. With potential derived charges, we aim at reproducing the electrostatic potential of pure silica framework as in zeolites with very low aluminum content. We determined PDC from BP-DF calculations on silica clusters (with dangling bonds saturated by hydrogen atoms, applying no external field), using the CHELP procedure[26] as implemented in the program Gaussian98.[27] Contacts of bond capping hydrogen atoms with tetrahedral Si atoms of the clusters result in unreasonably small PDC of Si atoms for pure silica framework; therefore, we designed all clusters such that only bonds dangling off oxygen centers were terminated by hydrogen centers. To derive PDC, we chose two pure-silica clusters, a 3T chain cluster (Figure 2a), and a four-ring (Figure 2b). We optimized each cluster structure, applying C_S and S_4 symmetry constraints, respectively, using a triple-ζ basis set augmented with polarization functions, TZV(d,p).[27] The same basis set was employed when determining potential derived charges. Two types of charges (one for silicon, Si, and one for oxygen, O_{Si}) are required to reproduce the electrostatic potential of a pure-silica lattice (Table 1). The corresponding FF parameters, q, to be used in the shell model description were chosen to preserve the neutrality of silica (SiO_2)

$$q(\text{Si}) + 2q(\text{O}_{\text{Si}}) = 0 \tag{13}$$

The PDC value of a Si atom, $q(\text{Si}) = 1.2e$, is compensated by the charges of two O centers, $q(\text{O}_{Si}) = -0.6e$. The PDC values for Si and O centers obtained here fall into the interval of 1.2 to 2.0e for $q(\text{Si})$ and -0.6 to $-1.0e$ for $q(\text{O})$, reported for periodic HF calculations with different basis sets.[2,3] The recent

TABLE 1: Electrostatic Potential Derived Charges (in *e*) Obtained from Gas-Phase Optimized Clusters

cluster[a]	PDC	
	O_{Si}	Si
$Si_3O_{10}H_8$[b]	−0.48	1.20
$Si_4O_{12}H_8$[c]	−0.48	1.11
final[d]	−0.6	1.2

[a] Calculations performed at BP-DF level with a TZV(d,p) basis set. [b] Linear cluster with three T-atoms (Figure 2a). [c] Four-membered ring (Figure 2b). [d] Chosen to represent the electrostatic field of extended systems.

embedding method of Sulimov et al.[11] uses higher charges for Si and O centers, 2.4 and −1.2 e, respectively, as proposed earlier by van Beest et al.[28]

3.2.2. Force Field. A shell model FF typically contains four interaction terms (see below). All centers treated at the MM level contribute to the Coulomb interaction ($V_{\text{Coul}}(R_{\text{lat}})$) as point charges (simple point charges representing cationic centers as well as cores and shells representing anionic centers)

$$V_{\text{Coul}} = \sum_{i,j} \frac{q_i q_j}{r_{ij}} \tag{14}$$

Closely connected to this term is the core−shell interaction ($V_{\text{core−shell}}$) that determines the polarizability of anionic centers, represented by a simple harmonic potential function (force constant k^{sh}) between core and shell of a given center i (O in the systems considered here)

$$V_{\text{core−shell}} = \sum_{i} k_i^{\text{sh}} \Delta r_i^2 \tag{15}$$

The remaining contributions to the FF are collectively described as short-range interactions. Typically, a Buckingham potential with both repulsive and attractive terms is used for pure silica and zeolite systems[29]

$$V_{\text{Buck}} = \sum_{i,j} [A_{ij} \exp(-r_{ij}/\rho_{ij}) - C_{ij} r_{ij}^{-6}] \tag{16}$$

However, in some force fields generated by fitting to data from HF or DF calculations, the attractive term is omitted with the argument that these methods are not able to properly account for dispersion interactions.[1] In those cases, nearest-neighbor bonding is represented only as Coulomb attraction of rather large charges (e.g., formal ionic charges).[1] Finally, there are three-body terms of the FF, connected with the stiffness of valence angles at T-atoms (Si, Al, Ti, etc.)

$$V_{\text{three−body}}(\theta) = \sum_{j=T} k_\theta (\theta_{ijk} - \theta_0)^2 \tag{17}$$

This term keeps the bond angles θ at all T-atoms in tetrahedral hybridization close to 109.47°; the summation runs over angles centered at T-atoms. It has been reported[30−32] that force field parametrizations based on small realistic charges require Si−O−Si three-body interaction terms for a correct description of bulk structural and physical properties. Alternatively to Si−O−Si three-body terms, two-body Si−Si terms have been used in some models.[30] Three-body terms analogous to eq 17 are included for the oxygen centers of the lattice.

Using the program GULP[33] for fitting BP-DF generated and some experimental reference data, we derived the parameters of a FF based on PDC. Our FF contains two pair-potential interactions, Si−O and O−O, and two interactions, O−Si−O

Covalent Oxides and Zeolites

J. Phys. Chem. B, Vol. 107, No. 10, 2003 **2233**

and Si—O—Si, of three-body type. The short-range interactions (except for the three-body term Si—O—Si) were parametrized using potential energy curves calculated for the 5T cluster Si-[OSi(OH)$_3$]$_4$. The value of the core—shell spring constant and the charges on core and shell of polarizable oxygen centers were fitted to reproduce changes of the dipole moment of the 2T cluster O[Si(OH)$_3$]$_2$ induced by a small point charge ($0.5e$) located at a distance of $\sim$20 au from the molecular center. The three-body Si—O—Si parameters were fitted to selected experimental data on structure and physical properties of two dense and three microporous silica materials (see below). Most parameters were determined in a two-step iterative procedure. First, the short-range interactions Si—O, O—O, and O—Si—O were parametrized. Then, the value of the core—shell harmonic spring and the corresponding charges of cores and shells for oxygen anions were optimized. Finally, after convergence was achieved for these iteratively determined parameters, the force constant for the three-body interaction Si—O—Si was established in a single step. After this overview of the parametrization procedure, we discuss some details.

To parametrize the pair potentials, Si—O and O—O, and the three-body interactions, O—Si—O, the geometry of the 5T model cluster was optimized at the BP level, using our standard basis sets (see computational details above) and applying a symmetry constraint according to the point group S_4. This symmetry restriction was preserved during the subsequent construction of potential energy curves. The potential energy curve for parametrizing the Si—O interaction was obtained in a pointwise fashion by stretching the Si—O bonds of the central tetrahedron of the 5T cluster from 1.40 to 1.95 Å (16 points), keeping the remaining internal coordinates fixed at their optimum values: r(Si—O) = 1.611 Å, $\angle$(O—Si—O) = 109.47°, $\angle$(Si—O—Si) = 158.8°. Similarly, the O—Si—O bending energy curve for deriving the O—O and O—Si—O parameters was constructed by varying two opposite O—Si—O angles from 80° to 140° (16 points), again keeping other structural parameters fixed at their equilibrium values: r(Si—O) = 1.622 Å in the central tetrahedron, r(Si—O) = 1.611 Å in the neighboring shell, $\angle$(Si—O—Si) = 158.8°. For each geometry of the target MM cluster (with fixed core positions of the ions), the shell positions of the anions were relaxed to equilibrium. The parameters of the three interactions Si—O, O—O, and O—Si—O are not independent: (i) the O—O bond length changes slightly when Si—O bond distances vary, and (ii) the short-range parameters describing the O—O and O—Si—O interactions are fitted to the same bending energy curve. For this reason, all these interactions were parametrized simultaneously.

To parametrize the anion polarizability, we performed BP-DF calculations for three configurations of the 2T cluster with the Si—O—Si angles set to 140°, 150°, and 160° and the Si—O and O—H bond lengths fixed at 1.647 and 0.971 Å, respectively. For a given geometry of the 2T cluster, the polarizability depends only on the shell displacement. Therefore, to obtain the core—shell parameters, we fitted the induced dipole moment of each 2T configuration calculated in the shell model approximation to the values determined in QM calculations.

Finally, the parameters of the Si—O—Si interaction were established. They were not fitted to calculated data, because Si—O—Si interactions in finite clusters and periodic systems are quite different. On the other hand, fitting to measured data only is also not adequate, as experimental Si—O bond distances,[34] 1.599—1.617 Å, are shorter than those calculated for the 5T reference cluster at the BP-DF level, 1.622 Å (see Table 2). Therefore, we followed a mixed strategy, using calculated

TABLE 2: Comparison of Optimized Structure Parameters (Bond Distances in Å, Bond Angles in deg) and Mulliken Charges (in e) of the Molecular Reference Cluster [(OH)$_3$Si—O]$_3$—Si—O—Si(OH)$_3$ Treated Fully Quantum Mechanically (a) and a Model Cluster with a OSi(OH)$_3$ Unit Substituted by an O* Pseudoatom and Point Charges^a (b)

parameter	**a**	**b**	deviation
r(Si1—O*)	1.622	1.621	0.001
r(Si1—O1)	1.622	1.618	0.004
r(Si1—O4)	1.622	1.625	0.003
r(Si2—O1)	1.611	1.611	0.000
r(Si2—O2)	1.649	1.650	0.001
r(Si2—O3)	1.650	1.653	0.003
$\angle$(O*-Si1—O1)	109.5	107.0	2.5
$\angle$(O1—Si1—O4)	109.5	111.5	2.0
$\angle$(O4—Si1—O4)	109.5	109.0	0.5
$\angle$(Si1—O1—Si2)	158.8	162.4	3.6
q(O*)	−0.78	−0.54^b	0.24
q(Si1)	1.64	1.45	0.19
q(Si2)	1.41	1.44	0.03
q(O1)	−0.78	−0.78	0.00
q(O2)	−0.67	−0.67	0.00
q(O3)	−0.67	−0.67	0.00
q(O4)	−0.78	−0.78	0.00

^{a} PDC values of PCs as used for the MM region (last row of Table 1). ^{b} Compensating charge of −0.282e at this center included.

TABLE 3: Force Field Parameters for PDC-Based BP-DF-Derived Shell-Model Potential

parameters		
charges	q(Si), e	1.2
	q(O$_{core}$), e	2.387
	q(O$_{shell}$), e	−2.987
short-range parameters	A (Si—O), eV	51431.799
	ρ (Si—O), Å	0.174872
	C (Si—O), eV Å^6	131.11
	A (O—O), eV	95169.354
	ρ (O—O), Å	0.1991
	C (O—O), eV Å^6	43.636
core—shell spring	k^{sh}, eV Å^{-2}	78.05
three-body interaction	k_θ (O—Si—O),^{a} eV rad^{-2}	0.89844
	k_θ (Si—O—Si),^{b} eV rad^{-2}	5.62

^{a} θ_0(O—Si—O) = 109.47°. ^{b} θ_0(Si—O—Si) = 163.4°.

as well as experimental data. The Si—O bond length, 1.622 Å, calculated for the 5T cluster was taken as one of the target quantities. Further target quantities, namely, structural data (cell parameters, Si—O—Si and O—Si—O bond angles) and other physical properties (elastic constants, bulk modulus, high-frequency dielectric constants) of two dense systems (α-quartz,[35,36] α-cristobalite[37]) and three microporous systems (zeolites chabazite CHA,[38] sodalite SOD,[39] and ZK-5[40]), were selected from experiment (see Tables 4 and 5).

The final parameters of our PDC-based FF are listed in Table 3. In Tables 4 and 5, we compare simulation results for the structure and other properties of crystalline reference materials with experiment and some well-known force fields for silica and zeolites.[1b,29] As can be seen from these tables, our PDC-based force field reproduces the experimental parameter with an accuracy comparable to widely used force fields. In addition, our FF has the advantage over alternative parametrizations in that it is based on realistic charges of the lattice centers that generate an adequate electrostatic field in zeolite cavities or close to a silica surface.

3.3. Partitioning of the Environment Region. To model an extended system like a zeolite, we partition the environment, region II, into three subregions:[8] (i) an inner region, IIa, surrounding the QM cluster, in which the positions of the ions, cores, and shells are explicitly optimized; (ii) an intermediate

TABLE 4: Comparison of Experimental Cell Parameters (in Å and deg) for Pure-Silica Dense and Microporous Polymorphs with Those Calculated with the New PDC-Based FF and Two Reference Force Fields

polymorphs		expt	present FF	empirical FF[g]	ab initio FF[h]
α-quartz[a]	$a = b$	4.913	4.896	4.84	4.99
	c	5.405	5.372	5.35	5.51
α-cristobalite[b]	$a = b$	4.978	5.004	4.97	5.13
	c	6.948	6.893	7.01	7.27
chabazite[c]	$a = b$	13.67	13.74	13.54	
	c	14.77	14.79	14.55	
sodalite[d]	$a = b = c$	8.848	8.848	8.82	8.95
ZK-5[e]	$a = b = c$	18.67	18.64		
faujasite[f]	$a = b = c$	24.26	24.64	24.23	24.63

[a] Reference 35. [b] Reference 37. [c] Reference 38b. [d] Reference 39. [e] Reference 40. [f] Reference 51. [g] Reference 29. [h] Reference 1b.

TABLE 5: Selected Physical Properties (Elastic Constants in 10^{10} N m^{-2}) of Dense Silica Polymorphs

	α-quartz				α-cristobalite	
	expt[a]	present FF	empirical FF[b]	ab initio FF[c]	expt	present FF
C_{11}	8.68	8.35	9.47	8.45	5.94	9.42
C_{12}	0.70	2.11	1.84	1.15	0.38	−0.52
C_{13}	1.91	1.82	1.97	2.39	−0.44	0.47
C_{14}	−1.80	−1.60	−1.45	−1.37	0.00	0.00
C_{33}	10.58	7.70	11.61	9.63	4.24	4.76
C_{44}	5.82	3.44	5.01	4.11	6.72	5.43
C_{66}	3.99	3.12	3.82	3.65	2.57	2.02
ϵ_{11}	4.45	2.10	4.74	4.07		
ϵ_{33}	4.81	2.12	5.01	4.42		
ϵ_{11}^{∞}	2.36	1.99	2.12	1.76		
ϵ_{33}^{∞}	2.36	2.02				
bulk modulus	36.9	39.8			16.0	25.3

[a] Reference 36. [b] Reference 29. [c] Reference 1b.
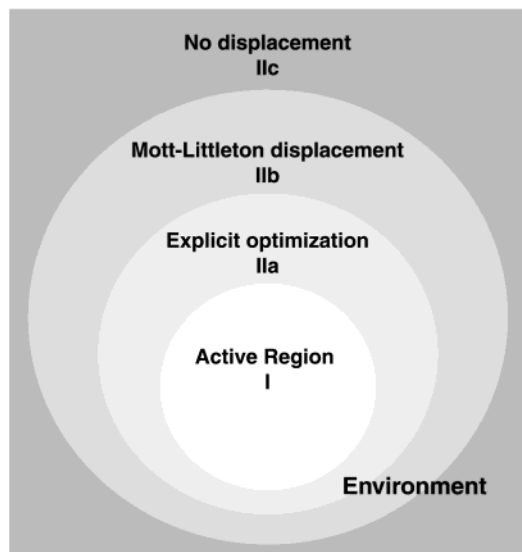
Figure 3. Partitioning of the environment region.

region, IIb, in which only an effective lattice polarization due to the effective charge of the defect is taken into account; and (iii) an outer region, IIc, in which the atomic positions are considered fixed, as in the unperturbed lattice (Figure 3). In regions IIa and IIb, the atomic structure of the polarized lattice is represented by an array of point charges and discrete dipoles (consisting of cores and shells). The effective polarization in region IIb is described by means of harmonic (Mott−Littleton) displacements of the ions from their equilibrium positions.[8,13]

TABLE 6: Optimized Pseudopotential Parameters of Capping Pseudoatoms O* for Different Angular Momentum Values l^a

l	n_l	α_l	A_l
0	0	7.599097	2.004069
1	0	19.87485	−0.242423
2	1	236.6773	1.514864

[a] See eq 18.

The remaining, outer part of the environment, region IIc, is considered as a dielectric medium, possibly polarized by a monopole located at the center of the QM region I. The polarization of this region contributes only to the energy of the defect but not to the forces acting on ions of the inner regions.

To represent the electrostatic potential of the environment on the QM cluster, the contribution of the neutral external part of the extended region IIc was substituted by that of a sphere that carries a surface charge density and encompasses the cluster. The radius was set at 15 au, and the surface charge density was represented by a finite set of 128 points. The values of the point charges were determined according to a procedure described previously.[9,41]

3.4. Parametrization of the Border Atoms. *3.4.1. Parametrization of the O* Pseudopotential.* As already mentioned in the Introduction, the optimization of parameters for border atoms saturating the dangling bonds of the quantum mechanical cluster is a key feature of the present embedding scheme. In our implementation, these border atoms are represented as monovalent atoms. For the present case of a silica environment, these border atoms are "pseudo"-oxygen centers O*, represented by a specially adjusted pseudopotential that is chosen in a form also used for nonlocal, angular-momentum-dependent effective core potentials[42]

$$V^{\text{eff}}(r) = V_L(r) + \sum_{l=0}^{L-1}[V_l(r) - V_L(r)]\sum_{m}|lm\rangle \langle lm|$$

$$V_l(r) = A_l r^{-n_l} \exp(-\alpha_l r^2) \qquad (18)$$

Here, l and m are the usual quantum numbers of eigenfunctions $|lm\rangle$ of the orbital angular momentum. L, set in our case at 2, represents the local part of the effective potential (see Table 6). The valence orbital basis as well as the initial parameters of the pseudopotential was taken from fluorine.[42] Recall that, as a functional element of the embedding scheme responsible for retaining proper charge balance, border atoms bear point charge increments, Δq_{pp}, which are half of the charge of oxygen atoms inside the MM region where these centers participate in two Si−O bonds (see section 2.1). In their embedding scheme for ionic−covalent systems,[11] Sulimov et al. assign effective charges to border atoms Si* in a similar way, 3/4 of the charge of standard Si centers.

We determined the pseudopotential parameters of the border atoms O* in a two-step iterative procedure. In the first step, we adjusted the parameters with a methodology similar to that described by Zhang et al.,[10b] targeting structural and electronic features of a model cluster (molecule) that has been treated fully quantum mechanically. Note an important aspect of our optimization strategy: the replaced moiety contains not only an O* pseudoatom but also the corresponding point charge increment, Δq_{pp}, and point charges representing the remainder of the substituted group. This procedure for fitting a cluster model corresponds more closely to the intended situation where a QM cluster with border pseudoatoms is embedded in a polar
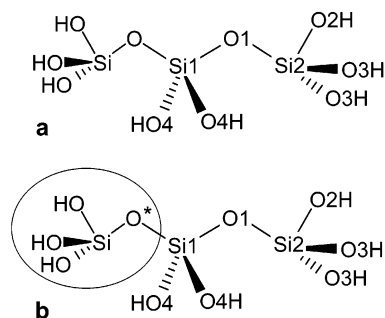
Covalent Oxides and Zeolites

J. Phys. Chem. B, Vol. 107, No. 10, 2003 **2235**

Figure 4. Sketch of the systems used for fitting the pseudopotential parameters: (a) reference system treated at the QM level and (b) system with a $OSi(OH)_3$ moiety substituted by point charges and an O* pseudopotential center represented in the form of a pseudoatom with one free valence.

environment, e.g., in silica or a zeolite. In the second step of the optimization procedure, we aimed at an improved representation of the electrostatic potential (ESP) of the embedded hybrid system. For this purpose, we compared the ESP of a QM cluster embedded in an array of point charges with the ESP of a periodic array of point charges that were located in lattice positions (e.g., of silica or a zeolite framework). To this end, we adjusted the charge increments Δq_{pp} of border pseudoatoms by redistributing charge to their Si neighbor in the MM region. The correction Δq_{pp}(Si) to the point charge of the Si center adjacent to an O* center aims at reproducing the electrostatic potential in the border region as accurately as possible (with atom-centered point charges) when compared to a periodic reference system. In this way, an eventual polarization of the O* centers due to neighboring Si centers can be modeled. However, the correction charge Δq_{pp}(Si) is only -0.018 e (see below); thus, O* centers are hardly polarized. After this optimization of Δq_{pp}(O*) and Δq_{pp}(Si), the pseudopotential parameters of O* were reoptimized (first step) and until changes in structural and electronic properties of the QM cluster or discrepancies in the electrostatic potential were reduced below a chosen threshold.

In the first step of the O* pseudopotential optimization, we used the QM cluster $(OH)_3Si-O-Si(OH)_2-O-Si(OH)_3$ (Figure 4a) as reference. One of the $O(Si(OH)_3)$ groups of this cluster was replaced by a pseudoatom O*, and the remaining atoms of the substituted $Si(OH)_3$ group were represented as point charges (Figure 4b). The point charges of the atomic centers of the substituent group $Si(OH)_3$ were taken at their potential-derived values, as in the molecular mechanics region of the embedding scheme (see section 3.2.1), i.e., $1.2e$ for silicon and $-0.6e$ for oxygen atoms. The charge of terminal hydrogen atoms of OH groups was set to $0.3e$, to preserve charge neutrality. According to bond-increment considerations (see section 2.1), a point charge $\Delta q_{pp} = 0.5 \times q(O_{MM}) = -0.3e$ was placed on the pseudoatom O*. By use of the simplex method, the O* pseudopotential parameters were optimized with the goal to reproduce the fully quantum mechanical results for structure and electron distribution of the QM part of the hybrid QM/MM cluster $(OH)_3Si-O-Si(OH)_2-O*$. Four characteristics of the reference system were chosen as the training set: the mean-square deviations of the potential energy curves of the bonds Si1−O* and Si1−O1 and the angle O1−Si1−O* (represented by a set of geometry configurations along these curves; Figure 5) as well as the square of the Mulliken charge difference of the atom Si1. The energy curves were constructed by changing the corresponding bond length or angle from the equilibrium value calculated for the reference system $(OH)_3Si-O-Si(OH)_2-O-Si(OH)_3$, keeping other internal coordinates at their
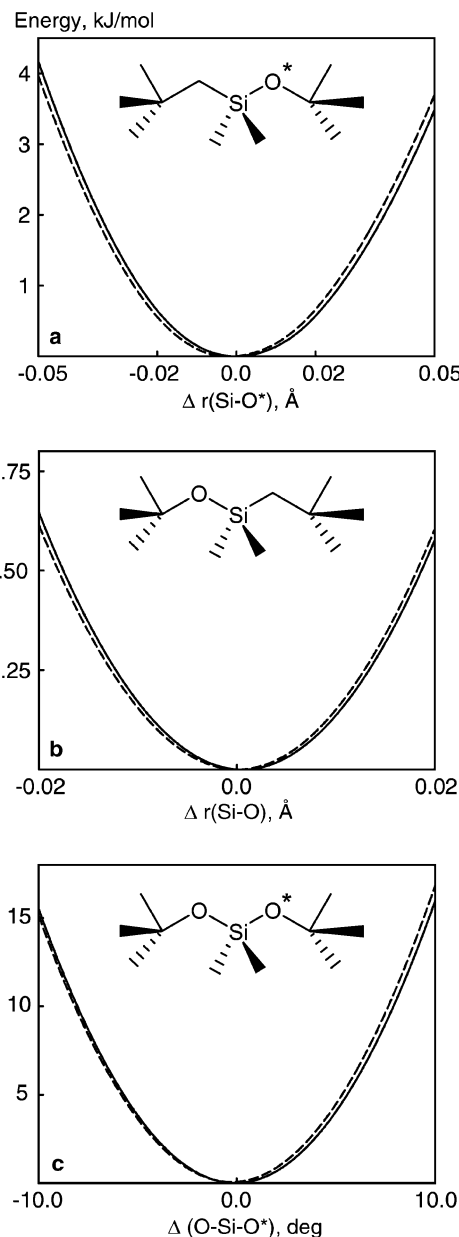
Figure 5. Comparison of various potential energy curves: (a) Si1−O* bond, (b) Si1−O1 bond, and (c) O1−Si1−O* angle in the systems shown in Figure 4; (a) (QM, dashed line) and (b) (QM/MM, solid line). The curves were obtained by varying the bond lengths Si1−O* (a), Si1−O1 (b), and the bond angle O1−Si1−O* (c), keeping all other internal coordinates fixed at their values optimized for system (a).

equilibrium value. The energy curves for the hybrid QM/MM system were obtained at analogous geometries. The mean-square deviations of each energy in au (5 points for the Si1−O* bond curve and 3 points for the Si1−O1 bond and the O1−Si1−O* angle curves) were weighted with a factor of 15, and the difference squared of the Mulliken charges (in e) was scaled with a factor of 0.005. The optimized O* pseudopotential parameters are listed in Table 6.

With a negative charge increment Δq_{pp} at the O* center, even after optimization of the effective O* pseudopotential on data pertaining to the reference Si1−O bond curve, the Si1−O* bond was reproduced notably too short. Therefore, we decided to introduce an additional compensating short-range repulsion between O* and Si1 centers

$$V(\{SiO\}*) = A_{ij} \exp(-r_{ij}/\rho_{ij}) \tag{19}$$

When optimizing parameters for O* centers, we gave priority to describing the charge distribution as well as the Si1−O bond adjacent to the pseudobond Si1−O* and the valence angle O1−Si−O*. Changes in these characteristics due to the pseudobond introduced reflect chemical effects of the substitution on properties of the unmodified QM moiety. We assume the QM cluster to be constructed in such a way that atoms of the pseudobond do not directly participate in chemical interactions of the active center of the cluster. Therefore, it is less important by which means mechanical characteristics of the pseudobond are reproduced. We fitted the short-range parameters A_{ij} and ρ_{ij} of the Si1−O* interaction once the pseudopotential parameters for the O* center were established, using the same 5T cluster $[(OH)_3SiO]_3Si−O−Si(OH)_3$ that had previously served for the parametrization of the short-range interactions of the PDC-based FF (section 3.2.2). The optimized pair-potential parameters (after convergence of the two-step iterative procedure) are $A_{ij}(\{SiO\}^*)$ = 10542.70 eV and $\rho_{ij}(\{SiO\}^*)$ = 0.1527 Å. In Figure 5, we see that the resulting bond stretching and bond angle energy curves obtained for the pure QM reference molecule and the corresponding hybrid QM/MM system agree very well.

In the second step of the optimization procedure, the QM cluster is embedded in its crystal environment, represented by an array of point charges. In the present case, we invoked a zeolite framework of chabazite structure containing only Si T-atoms. The QM model cluster was constructed by substituting an $O_3SiOSiO_3$ fragment of the periodic system by the cluster $O^*_3SiOSiO^*_3$ to be treated quantum mechanically. The O* pseudopotential parameters were set to the values determined in the preceding step. Then, the charges $\Delta q_{pp}(O^*)$ and Δq_{pp}-(Si) were optimized by fitting the ESP of the hybrid QM/MM system to the ESP of the periodic array of potential-derived charges by a least-squares technique using a grid of 2500 points distributed around the center of an 8T ring (Figure 6). We started the optimization from a situation where the charge Δq_{pp} is fully localized on the core of the border pseudoatoms O*, i.e., $\Delta q_{pp}(O^*) = -0.3e$ and $\Delta q_{pp}(Si) = 0e$. The iterative fitting procedure converged after three cycles to $\Delta q_{pp}(O^*) = -0.282e$ and $\Delta q_{pp}(Si) = -0.018e$.

Thus far, we tested the parametrization of the O* pseudopotential on clusters with fixed geometries. Bond lengths, bond angles, and Mulliken charges had been optimized for the QM cluster in the gas phase. In Table 2, we compare these values to those obtained for the hybrid QM/MM system. Si−O bond distances of the two systems deviate at most by 0.004 Å. The Si−O* pseudobond is 0.001 Å shorter than the corresponding Si−O bond of the QM system, and the bond distances Si1−O1 and Si1−O4 closest to the pseudobond bond deviate by 0.004 and 0.003 Å, respectively, from the corresponding quantities of the 5T gas-phase cluster $[(OH)_3SiO]_3Si−O−Si(OH)_3$ treated fully quantum mechanically. Other bond distances differ less than 0.003 Å. O−Si−O bond angles of both molecular systems agree to 4°. Discrepancies of Mulliken charges are almost negligible (0.01−0.03e), except for the O center to be replaced by the pseudoatom O* and the center Si1 next to O*; these charges differ by 0.24 and 0.19e, respectively.

In Figure 6, we compare electrostatic potential maps for a periodic array of PDCs, and the QM cluster embedded in an array of point charges with modified charges $\Delta q_{pp}(O^*)$ and Δq_{pp}-(Si) (see above). The largest difference of the two ESP maps occurs close to the border pseudoatom O*. There, the ESP of the QM/EPE system is 0.02 au more positive than the ESP of the purely MM reference structure. Nevertheless, the electrostatic potential is well reproduced close to oxygen centers where
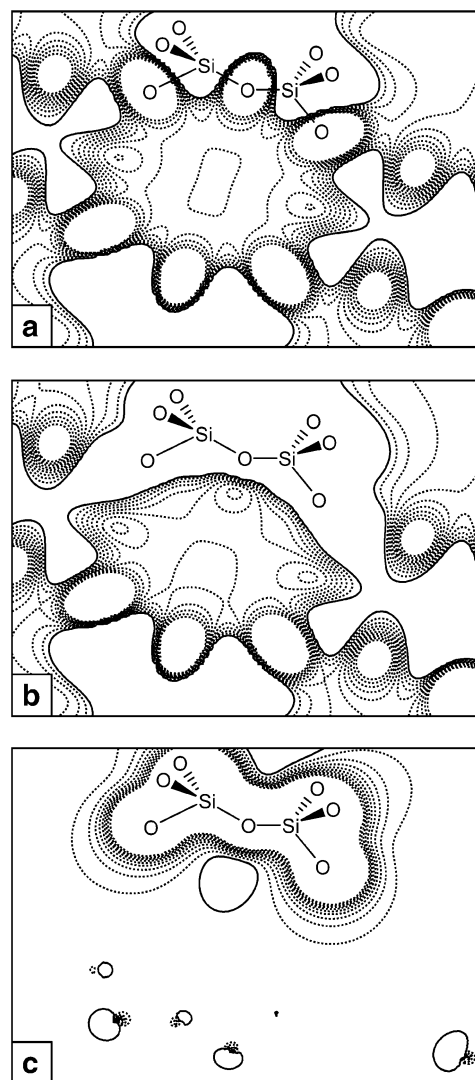

Figure 6. Electrostatic potential (ESP) maps for (a) an array of point charges located in positions of lattice atoms of a chabazite framework, (b) the hybrid QM/MM system where a 2T QM cluster is embedded in an array of point charges, and (c) the difference of ESPs between (a) and (b). Dashed and solid contours correspond to negative and positive ESP values, respectively. The contours represent equidistant values with an increment of 0.009 au (23.6 kJ/mol).

acidic protons are to be attached after substitution of Si with Al to model active centers of aluminosilicates. Therefore, we do not expect these differences in the ESP to affect OH vibrational frequencies, deprotonation energies, and other chemical properties of the active site in a crucial fashion (see section 4).

3.4.2. Parametrization of the Pair Potential for QM/EPE Coupling. Thus far, we focused on the parametrization of border pseudoatoms O* which are responsible for reproducing of the internal structure of the embedded quantum mechanical cluster. Finally, we need to address pair potential parameters for the interaction of the QM cluster with its MM environment; see the interaction of O*−Si(MM) in Figure 1. This interaction is responsible for the correct orientation of the QM cluster in the cavity formed in the MM lattice.

We parametrized pair-potential parameters for the QM/EPE linking analogously to the procedure utilized for the O* pseudopotential. As before, we used the 5T model system $[(OH)_3SiO]_3Si−O−Si(OH)_3$, where the moiety $[(OH)_3SiO]_3Si−O^*$ was treated quantum mechanically and the "missing" Si-

Covalent Oxides and Zeolites

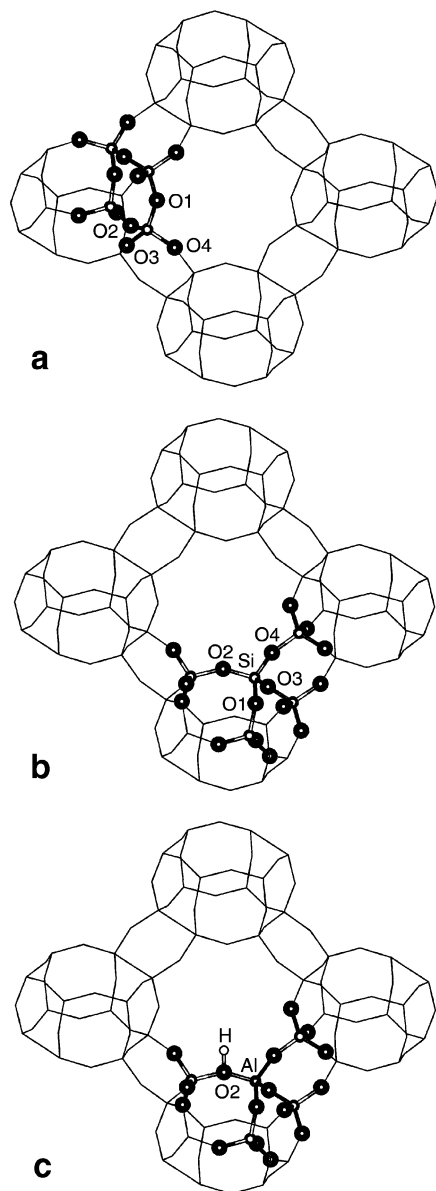*J. Phys. Chem. B, Vol. 107, No. 10, 2003* **2237**

Figure 7. Structures of embedded zeolite clusters used in the simulation of chabazite: (a) four-ring of pure-silica chabazite, 4T QM cluster; (b) pure-silica 5T QM cluster where the crystallographic positions of the O atoms are specified as given in ref 34; (c) Al-containing 5T QM cluster with an OH group in position O2. The atoms of the QM cluster are shown as open circles.

$(OH)_3$ moiety was represented by potential-derived charges (O = $-0.6e$, Si = 1.2 e, H = $0.3e$). A pair potential for the O*−Si(MM) interaction, again of Buckingham type, eq 16, was adapted such that the Si−O potential energy curve, calculated previously (section 3.2.2), was reproduced. We obtained the following optimized parameters for the QM/EPE coupling: A_{ij} = 36739.265 eV, ρ = 0.2031 Å, C = 296.26 eV·Å^6 (cf. Table 3).

4. Application of the covEPE Method to Zeolites

As the first application of the new embedding scheme for systems with directional covalent bonds, we studied the structures of pure-silica and H-chabazite as well as the OH vibrational frequencies and deprotonation energies of the latter material. We calculated structural parameters of pure-silica chabazite for two QM model clusters: 4T, representing a four-ring (Figure 7a) and 5T, with a central Si center surrounded by

TABLE 7: Calculated and Experimental Structure Parameters (Bond Distances in Å, Bond Angles in deg) of Pure-Silica Chabazite[a]

	QM/EPE		MM	PW[e]	exp[f]
	4T[b]	5T[c]	present FF[d]		
r(Si−O1)	1.635, 1.638	1.640	1.625	1.616	1.617
	1.640, 1.642	1.646			
r(Si−O2)	1.638, 1.639	1.629, 1.653	1.624	1.605	1.599
r(Si−O3)	1.640, 1.641	1.641, 1.644	1.627	1.612	1.615
r(Si−O4)		1.622, 1.649	1.625	1.612	1.613
∠(O1−Si−O2)	110.2, 110.3	109.4	111.8	109.7	110.3
∠(O1−Si−O3)	109.6, 109.7	110.0	110.2	109.0	110.2
∠(O1−Si−O4)		109.7	108.0	111.8	107.9
∠(O2−Si−O3)		109.1	107.7	109.5	109.7
∠(O2−Si−O4)		110.2	107.8	107.9	108.4
∠(O3−Si−O4)		108.3	111.3	108.9	110.2
∠(Si−O1−Si)	150.8, 151.0	148.1	148.3	154.1	144.8
∠(Si−O2−Si)	149.6	150.5	147.4	150.6	149.4
∠(Si−O3−Si)	147.5	146.5	147.4	150.2	147.8
∠(Si−O4−Si)		151.4	145.8	144.1	150.0

[a] Only the structure of the QM part of the QM/EPE system is given. [b] Structure in Figure 7a. [c] Structure in Figure 7b. [d] Present work. [e] Plane-wave (PW) calculation (supercell approach, Perdew−Wang exchange-correlation potential); ref 43. [f] Reference 34.

four OSiO*$_3$ groups (Figure 7b). The 5T model was also used to model an Al-containing H-chabazite (Figure 7c). The covEPE environment of the QM clusters was described by the newly parametrized force field based on PDC charges. The QM part of the system (region I) consists of 16−22 atoms, regions IIa and IIb contain 381−416 and 2485−2640 centers, respectively, and region IIc is assumed to be unlimited. In the following section, we compare the results obtained with those of other theoretical studies (MM, QM, and QM/MM) and experimental data where available.

4.1. Structure. *4.1.1. Pure-Silica Structures.* The pure-silica chabazite structure features one kind of tetrahedral (Si) position and four kinds of oxygen positions,[34] O1, O2, O3, and O4 (Figure 7). Therefore, in chabazite, there are four different types of Si−O bonds, six types of tetrahedral O−Si−O angles, and four types of Si−O−Si angles. In Table 7, we present these structure parameters as calculated with the QM/EPE embedding approach for 4T and 5T quantum mechanical clusters. The structure data determined in periodic plane-wave calculations[43] and in experiment[34] are also given for comparison. Furthermore, we list the structure parameters obtained in a MM simulation with the PDC-based force field established in this work (Table 7). The geometrical parameters obtained in the QM/EPE calculations for the 4T and 5T QM clusters are found close each to other, agreeing within 0.01 Å and 1−3°. However, bond distances and angles in the QM part of hybrid QM/EPE systems vary slightly, depending on their distance to the QM/EPE border (Table 8). For example, three regions can be distinguished in the 5T cluster: (i) the first shell farthest from the QM/EPE border, containing the central SiO$_4$ tetrahedra, (ii) the second shell next to the first region comprising one shell of Si centers, (iii) the third shell closest to the QM/EPE border containing the pseudoatoms O*, and (iv) the QM/EPE border region, which includes the O*−Si(MM) bonds and the bond angles O*−Si-(MM)−O(MM), O*−Si(MM)−O*, and Si−O*−Si(MM).

The Si−O bond lengths of the first and second shells of the 5T cluster vary in the ranges 1.622−1.641 and 1.644−1.653 Å, respectively (Table 8). The bonds of the second shell are longer than those of the first shell; moreover, the shorter the Si−O bonds of the innermost shell, the longer the corresponding Si−O bonds in the second shell. The bonds on the QM/EPE

TABLE 8: Optimized Structure Parameters (Bond Lengths in Å, Bond Angles in deg) from Hybrid QM/EPE Embedded Calculations on the 5T Cluster $Si(OSiO_3)_4$ in a Chabazite Environment (Figure 7b)

| | MM | QM cluster | | | QM/EPE links |
		first shell	second shell	third shell[a]	
r(Si$-$O)	1.624$-$1.627	1.622$-$1.641	1.644$-$1.653	1.629$-$1.642	1.630$-$1.637
$\angle$(O$-$Si$-$O)	107.8$-$111.8	108.3$-$110.2	105.5$-$113.1	105.3$-$113.6	103.1$-$113.2
$\angle$(Si$-$O$-$Si)	145.8$-$148.3	146.5$-$151.4		140.3$-$146.7	

[a] Including O* centers.

border—the pseudobonds Si$-$O* and the QM/EPE links O*-Si(MM)—agree well with the Si$-$O bond lengths of the first shell of the QM part of the QM/EPE system. The Si$-$O bond lengths of the two shells of the hybrid 5T-QM/EPE systems agree with those of the corresponding force field results, with maximal deviations of 0.015 and 0.029 Å, respectively. In the present QM/EPE calculations, bond lengths are overestimated compared to experiment, just as in other generalized gradient approximation (GGA) calculations (see above).[21] It appears that the bond lengths of periodic plane-wave GGA calculations[43] are shorter than the true GGA limit,[25,48] probably as a consequence of the specific type of pseudopotentials used.

Similar to the bond distances, results of O$-$Si$-$O angles depend on their location relative to the QM/EPE border. O$-$Si$-$O angles of the central tetrahedron of the QM cluster fall into the narrow interval 108$-$110°, whereas the differences between the tetrahedral angles of subsequent shells and at the QM/EPE border exceed 10°; the values are between 103° and 114° (Table 8). The O*$-$Si(MM)$-$O* angles, 118°, deviate more from the ideal tetrahedral angle; this can be rationalized by the fact that the embedded QM cluster is somewhat larger than its MM counterpart of the chabazite lattice due to longer Si$-$O bonds calculated at the GGA level.

The Si$-$O$-$Si angles obtained for the QM part of hybrid QM/EPE system fall into the interval 147$-$151°, in very good agreement with experimental values,[34] 145$-$150°, and results of our molecular mechanic calculations, 146$-$148° (Table 7). The Si$-$O*$-$Si(MM) angles, calculated at 140$-$147°, are about 4$-$7° smaller than Si$-$O$-$Si angles in the QM part of the system.

4.1.2. Al-Containing Structures. As a model for Brønsted acid sites in zeolites, we studied Al-containing chabazite. An Al-exchanged structure is modeled by substituting the central Si atom of the 5T QM cluster by an Al center (Figure 7c), while the EPE environment is considered as pure-silica. The model system constructed in such a way corresponds to a zeolite with a very high Si/Al ratio, more than 1000 Si atoms in the regions I, IIa, and IIb, per only one Al. Four different protonated forms of the $(O_3SiO)_3Al-O(H)-SiO_3$ cluster were studied, with the proton attached to each of the four crystallographic oxygen centers.[34] The structure parameters obtained from embedded QM/EPE calculations for deprotonated and protonated forms of Al-containing chabazite are presented in Table 9. Geometrical changes are most significant in the region close to the central Al impurity and decrease with increasing distance from this center. The T$-$O bonds of the central TO_4 tetrahedron of the deprotonated cluster $Al(O_3SiO)_4{}^-$ (Al0 in Table 9) are calculated to be stretched by 0.11$-$0.13 Å compared to the corresponding pure Si cluster. The Al$-$O bond distances are calculated from 1.736 to 1.769 Å. The Si$-$O bond lengths of the second shell of the QM cluster $Al(O_3SiO)_4{}^-$ fall into the interval 1.596$-$1.602 Å; they are 0.04$-$0.05 Å shorter than those in the pure-silica structure. Bond length changes in the third shell of the Al-containing QM cluster relative to the corresponding silica cluster are even smaller than those in two inner shells; they do

TABLE 9: Optimized Structure Parameters (Bond Lengths in Å, Bond Angles in deg) of 5T Pure-Silica (Si) and Al-Containing Clusters[a] Embedded in a Chabazite Framework

	Si	AlO[b]	Al(O1H)	Al(O2H)	Al(O3H)	Al(O4H)
r(T$-$O1)	1.640	1.763	1.952	1.716	1.720	1.724
r(T$-$O2)	1.629	1.754	1.712	1.925	1.722	1.717
r(T$-$O3)	1.644	1.769	1.729	1.726	1.943	1.730
r(T$-$O4)	1.622	1.736	1.716	1.729	1.698	1.911
r(O$-$H)			0.977	0.981	0.980	0.977
r(Si$-$O1)	1.646	1.602	1.706	1.619	1.618	1.618
r(Si$-$O2)	1.653	1.599	1.624	1.716	1.623	1.628
r(Si$-$O3)	1.641	1.602	1.622	1.626	1.705	1.629
r(Si$-$O4)	1.649	1.596	1.631	1.637	1.621	1.728
$\angle$(O1$-$T$-$O2)	109.4	106.6	100.1	102.3	115.0	112.4
$\angle$(O1$-$T$-$O3)	110.0	109.4	101.9	115.5	102.0	115.1
$\angle$(O1$-$T$-$O4)	109.7	110.6	94.5	118.0	115.1	104.0
$\angle$(O2$-$T$-$O3)	109.1	110.9	116.5	108.1	95.0	120.7
$\angle$(O2$-$T$-$O4)	110.2	112.1	120.6	93.8	123.0	102.3
$\angle$(O3$-$T$-$O4)	108.3	107.3	116.1	115.1	99.5	98.7
$\angle$(H$-$O$-$Al)			107.5	102.6	109.2	112.1
$\angle$(H$-$O$-$Si)			116.4	114.6	120.0	111.5
$\angle$(T$-$O1$-$Si)	148.1	150.1	135.3	150.3	145.1	152.6
$\angle$(T$-$O2$-$Si)	150.5	153.4	157.7	141.0	156.2	144.2
$\angle$(T$-$O3$-$Si)	146.5	142.4	139.8	137.6	130.5	137.9
$\angle$(T$-$O4$-$Si)	151.4	152.7	154.7	144.3	179.7	136.4

[a] The numbering refers to the different positions of oxygen atoms to which a proton is attached; see Figure 7b. [b] Deprotonated cluster.

not exceed 0.011 Å. The Si$-$O bonds at the QM/EPE border of the Al-containing system were calculated to be shorter than those in the Al-free systems, but the changes are less than 0.01 Å. In general, T$-$O bond length changes alternate in subsequent shells, in agreement with the principle of bond order conservation as previously reported for zeolites.[43,44]

Substitution of a Si center by an Al atom also affects the O$-$T$-$O angles in the central tetrahedron TO_4 of the charged QM cluster $Al(O_3SiO)_4{}^-$. O$-$Al$-$O angles vary with a larger amplitude, 106.6$-$112.1°, compared to O$-$Si$-$O angles, 108.3$-$110.2°, of the corresponding SiO_4 tetrahedron of pure-silica systems. Note that three of the six O$-$Al$-$O angles are larger, and the remaining three are smaller than the ideal tetrahedral angle. The O$-$Si$-$O angles in the second shell of the Al-containing system, 105.9$-$115.2°, and the tetrahedral angles in the third shell, 103.6$-$111.2°, are almost unchanged from the corresponding angles in pure-silica systems (not shown in tables). The angles O*$-$Si(MM)$-$O(MM) at the QM/MM border vary in the range 99.5$-$113.7° As for pure-silica structures, O*$-$Si(MM)$-$O* angles deviate significantly (127$-$130°) from the tetrahedral angles in the inner parts of the QM cluster.

The Al$-$O$-$Si angles connecting two atoms in tetrahedral positions obtained for the QM part of the charged QM cluster $Al(O_3SiO)_4{}^-$ range from 142° to 153°. The Si$-$O*$-$Si(MM) angles are 134$-$142°, i.e., they are smaller than analogous angles in Al-free systems. This compression of Si$-$O*$-$Si(MM) angles is a consequence of the larger size of the QM cluster due to the substitution of the central silicon atom by an aluminum impurity.

As expected, attachment of a proton H$^+$ to a specific oxygen center of the QM cluster results in an extension of the

Covalent Oxides and Zeolites

J. Phys. Chem. B, Vol. 107, No. 10, 2003 **2239**

TABLE 10: Calculated and Experimental OH Frequencies (in cm^{-1}) of a Bridging OH Group in Chabazite at the Four Crystallographic O Positions^{a,b}

QM method	model	Si:Al	O1	O2	O3	O4
expt^c		16:1	3603	3579		
BP	QM/EPE^d	>1000	3586	3546	3561	3609
PW	plane-wave^{e,f}	11:1	3675	3720	3620	3615
PW	plane-wave^{e,g}	11:1	3590	3565	3570	3580
PW	plane-wave^{e,h}	11:1	3574	3555	3557	3545
B3LYP	periodic^{e,i}	1:1	3669			
B3LYP	QM-Pot^{e,j}	11:1	3684			
BP	isolated-2T^k			3459		
BP	isolated-3T^l			3565		
B3LYP	isolated-8T^m			3737		

^{a} Harmonic frequencies are reported for BP calculations of isolated clusters with QM/EPE; the other calculated values represent anharmonic frequencies. Also given is the Si:Al ratio of the system or model used. ^{b} The numbering refers to the different positions of oxygen atoms to which a proton is attached; see Figure 7b. ^{c} Reference 34. ^{d} Present calculation; for the ratio Si:Al > 1000 see section 4.1.2. ^{e} Anharmonicity corrected values. ^{f} Reference 47. ^{g} Reference 46. ^{h} Reference 43. ^{i} Reference 45. ^{j} Reference 1c. ^{k} Reference 49. ^{l} Reference 25. ^{m} Eight-ring; ref 48.

corresponding Al−O(H) and Si−O(H) bonds by about 0.20 and 0.10 Å, respectively, compared to the deprotonated Al-containing cluster Al0 (Table 9). The other Al−O distances of the QM cluster are contracted by 0.02−0.05 Å. The lengths of the Al−O(H) and Si−O(H) bonds vary slightly with the position of the OH group at one of the four crystallographic oxygen sites (by 0.04 and 0.02 Å, respectively). Similar variations were observed in periodic plane-wave[43] and QM-Pot[1e] calculations. The O−H bond length is 0.979 ± 0.002 Å, depending on the position of the proton. These calculated values are close to the results of periodic plane-wave[43] calculations employing the Perdew-Wang (PW) functional, 0.975 ± 0.001 Å, and of periodic B3LYP modeling,[45] 0.968 Å (for Si/Al = 1), whereas the QM-Pot approach at the HF level[1e] yields shorter O−H bonds, 0.955 Å.

The presence of a bridging OH group in the protonated clusters and changes in the bond lengths close to the OH group cause substantial alterations of the bond angles. The Al−O(H)−Si angles, 130−141°, are 12−16° smaller than those in the deprotonated cluster. Similar values of these bond angles were found in periodic PW and QM-Pot calculations.[1e,43] The angles at the central Al atom also deviate from the tetrahedral reference; two of them are smaller and the other two larger (Table 9).

4.2. Frequencies. In Table 10, we report calculated OH harmonic frequencies, and we compare our results with experimental data[34] and OH frequencies obtained in periodic PW plane-wave simulations,[43,46,47] periodic B3LYP modeling,[45] the QM-Pot embedding approach,[1c] and gas-phase cluster calculations.[48] In general, the calculated values of the OH frequencies vary considerably between the different computational methods. Moreover, even the same models and computational approach (e.g., the PW plane-wave calculations[43,46,47]) can yield values that differ by more than 100 cm^{-1} (Table 10). The O−H frequencies calculated with our QM/EPE method range from 3546 to 3609 cm^{-1}, close to the experimental values 3579−3603 cm^{-1}.[34]

It has previously been noted that harmonic frequencies calculated with the LCGTO−FF−DF method using the BP exchange-correlation functional agree closely with experimental vibrational frequencies of O−H and other bonds.[25,49,50] When comparing to experiment, note that the latter was performed on a sample with a ratio of Si/Al = 16, while our model system corresponds to a ratio of Si/Al > 1000. As previously discussed,[45] the OH frequency decreases with increasing Si/Al

TABLE 11: Calculated Deprotonation Energies (DE) and Relative Stabilities ΔE^a (in kJ/mol) of OH Groups in Chabazite at Four Crystallographic O Positions

QM method	model		O1	O2	O3	O4
BP	QM/EPE^b	DE	1250	1256	1251	1258
		ΔE		−6	−1	−8
HF	QM-Pot^c	DE	1277	1258	1266	1255
		ΔE		19	11	22
HF	periodic/QM-Pot^{c,d}	ΔE		17	13	13
BP	isolated-2T^e	DE		1271		
PW	plane-wave^f	ΔE		5	6	9
PW	plane-wave^g	ΔE		7	4	9

^{a} Relative to that of position O1. ^{b} Present calculation. ^{c} Reference 1e. ^{d} Single-point energy calculated with a periodic HF method at structures obtained with the QM-Pot method. ^{e} Reference 49. ^{f} Reference 43. ^{g} Reference 47.

ratio. From this effect, we expect some increase of our calculated OH frequencies for the ratio Si/Al = 16, closer to the experimental frequency values. The available experimental information for the OH frequency of the hydroxyl groups at O1 and O2 oxygen positions in chabazite, 3603 and 3579 cm^{-1},[34] allows a direct comparison with our results, which are only 19−33 cm^{-1} smaller than the experimental values for the corresponding position (Table 10). The higher frequency of the OH group in O1 position is also semiquantitatively predicted, calculated by 40 cm^{-1}, and in experiment by 24 cm^{-1}.[34] The accuracy of the BP QM/EPE calculations is comparable with more recent PW plane-wave calculations,[43,46] where the difference between calculated and experimental values was 13−29 cm^{-1}. Earlier plane-wave simulations[47] yielded a considerably higher OH frequency than that obtained by experiment (>70 cm^{-1}); moreover, the OH frequency at the O2 position was calculated to be 45 cm^{-1} larger than that obtained at the O1 position, at variance with experimental observations (Table 10). The QM-Pot calculation with the B3LYP method[1c] yielded an OH frequency that is 81 cm^{-1} larger than the experimental value. Periodic B3LYP modeling[45] also gives a high value of the OH frequency; however, this value applies to a system with a ratio of Si/Al = 1. Unfortunately, we cannot compare to OH values for other Si/Al ratios reported in ref 45, because the corresponding structures were optimized at MM level only. The frequencies obtained in plane-wave, QM-Pot, and periodic B3LYP calculations are corrected for anharmonicity effects, at variance with the present QM/EPE calculations. In summary, compared to other available contemporary methods, the OH frequencies at different positions in chabazite calculated here with our QM/EPE approach agree well with experiment. In part, this good correspondence is due to a compensation of the missing anharmonicity corrections and the underestimation of OH frequencies by the BP functional.[25,49,50]

4.3. Deprotonation Energies. The deprotonation energies (DEs) of the hydroxyl groups in chabazite calculated with the QM/EPE method vary between 1250 and 1258 kJ/mol (Table 11). These results cannot be compared with experiment, because DEs are not amenable to direct measurement. Also, supercell calculations are not suitable for modeling the deprotonated form of a zeolite, because it represents a charged defect in a periodic structure. Therefore, our results can be compared only with those from other QM/MM embedding methods and QM gas-phase cluster models.[1,49] Quantum mechanical calculations of DE using isolated cluster models yield values from 1200 to 1400 kJ/mol, depending on the QM method, the basis set, and the cluster size.[5] An earlier computational study of our group[49] at the BP level on an isolated 2T cluster furnished a deprotonation energy of 1271 kJ/mol, i.e., a slightly higher value than the DE obtained

with the present covEPE embedding method. Our present results are close to DE values obtained with the QM-Pot method at the HF level[1e] (Table 11); the differences are between 3 and 27 kJ/mol for different positions of the OH group. However, in the calculations of Brändle et al.,[1e] the DE varied by 22 kJ/mol for different crystallographic oxygen positions, whereas the DE values of the present work vary by 8 kJ/mol only. This different behavior could be due to the way the electrostatic field of the framework on the active site is represented in both embedding techniques. Recall that the covEPE method takes long-range electrostatic effects fully into account, at variance with the QM-Pot approach, which includes such field effects only at the MM level. Alternatively, the difference could originate from different levels of theory used in the two calculations, HF and BP-DF, respectively.

Because all four protonated structures in our model have the same deprotonated form, $Al(O_3SiO)_4^-$, differences in DE can also be connected with the relative stabilities of the corresponding sites. Table 11 shows the relative stabilities (ΔE) of the four positions of bridging OH groups, using structure O1−H as reference. As can be seen, the stability of the four sites is very similar, within 8 kJ/mol, similar to results of plane-wave calculations at the PW level, which yielded a stability range of 9 kJ/mol.[43,47] As already discussed,[43] these small differences in relative stability are quite close to the accuracy limits of the computational methods used and to thermal energies, e.g., the situation in a zeolite can deviate from the calculated order of stability. The order of stability obtained in the present study, O4 > O2 > O3 > O1, does not agree with other computational approaches. Plane-wave supercell calculations furnished the ranking O1 > O2 > O3 > O4.[43] The QM-Pot approach suggests similar ordering, but with more than twice larger differences between the most and the least favored positions, 22 kJ/mol.[1e]

5. Conclusions

In the present paper, we reported a density functional based implementation of a combined QM/MM approach for covalent oxides and zeolites. This procedure is an adaptation of the EPE cluster embedding scheme for the description of surfaces of ionic systems, previously developed by us.[8] The EPE formalism accounts for the lattice relaxation around a quantum mechanical cluster in response to changes in its geometry and electron (re)-distribution. The present covEPE implementation affords a smooth embedding of the cluster in its environment due to a specially parametrized force field for simulating the classical environment. This force field was derived from calculated data, obtained at the same theoretical level as used for the quantum mechanical cluster, and physically meaningful charges to represent the atomic centers.

With this embedding scheme, we investigated the local structure, the OH vibrational frequencies, and the deprotonation energies of four different acidic sites in chabazite with very low loading (Si/Al > 1000) of aluminum centers. We also studied the effect of substituting a regular silicon center by an aluminum impurity on the local geometry of the lattice. Insertion of an Al atom was found to induce a significant perturbation of the structure in two neighboring shells around the impurity; changes in shells farther away are less than 0.01 Å. The calculated OH vibrational frequencies reflect the differences in the structure of the acidic sites and agree well with experimental values. Anharmonicity effects (typically[43−47] about 150−200 cm^{-1}) are not included in the present results, and the close correspondence of calculated and experimental vibrational frequencies is, to the extent just mentioned, due to error

compensation of our BP calculations. The deprotonation energies of different crystallographic sites of the OH group were calculated to vary by less than 1%; the values obtained are similar to results of previous theoretical studies.

The covEPE cluster embedding scheme introduced here is applicable for exploring silica systems with different impurities, e.g., framework substituted transition metal atoms such as Ti, V, and Fe. The covEPE embedding accounts for long-range electrostatic interactions of the centers in the QM cluster with its classical surrounding and thus allows us to study, in an accurate way, how chemical modifications of the environment affect characteristics of a reactive center.

References and Notes

(1) (a) Eichler, U.; Kölmel, C. M.; Sauer, J. *J. Comput. Chem.* **1996**, *18*, 463. (b) Schröder, K.-P.; Sauer, J. *J. Phys. Chem.* **1996**, *100*, 11043. (c) Sierka, M.; Sauer, J. *Faraday Discuss.* **1997**, *106*, 41. (d) Brändle, M.; Sauer, J. *J. Am. Chem. Soc.* **1998**, *120*, 1556. (e) Brändle, M.; Sauer, J.; Dovesi, R.; Harrison, N. M. *J. Chem. Phys.* **1998**, *109*, 10379. (f) Sauer, J.; Sierka M. *J. Comput. Chem.* **2000**, *21*, 1470.

(2) (a) Sherwood, P.; de Vries, A.; Collins, S. J.; Greatbanks, S. P.; Burton, N. A.; Vincent, M. A.; Hiller, I. H. *Faraday Discuss.* **1997**, *106*, 79. (b) de Vries, A.; Sherwood, P.; Collins, S. J.; Rigby, A. M.; Rigutto, M.; Kramer, G. J. *J. Phys. Chem.* **1999**, *103*, 6133.

(3) (a) Greatbanks, S. P.; Sherwood, P.; Hiller, I. H. *J. Phys. Chem.* **1994**, *98*, 8134. (b) Greatbanks, S. P.; Hiller, I. H.; Burton, N. A.; Sherwood, P. *J. Chem. Phys.* **1996**, *105*, 3770. (c) Teunissen, E. H.; Jansen, A. P. J.; van Santen, R. A. *J. Phys. Chem.* **1995**, *99*, 1873. (d) Kyrlidis, A.; Cook, S. J.; Chakraborty, A. K.; Bell, A. T.; Theodorou, D. N. *J. Phys. Chem.* **1995**, *99*, 1505. (e) Vollmer, J. M.; Stefanovich, E. V.; Truong, T. N. *J. Phys. Chem. B* **1999**, *103*, 9415.

(4) Lopez, N.; Pacchioni, G.; Maseras, F.; Illas, F. *Chem. Phys. Lett.* **1998**, *294*, 611.

(5) (a) Sauer, J.; Ugliengo, P.; Garrone, E.; Saunders, V. R. *Chem. Rev.* **1994**, *94*, 2095. (b) Bates, S. P.; van Santen, R. A. *Adv. Catal.* **1998**, *42*, 1.

(6) (a) Maseras, F.; Morokuma, K. *J. Comput. Chem.* **1995**, *16*, 1170. (b) Matsubara, T.; Sieber, S.; Morokuma, K. *Int. J. Quantum Chem.* **1996**, *60*, 1101. (c) Svensson, M.; Humbel, S.; Morokuma, K. *J. Chem. Phys.* **1996**, *105*, 3654.

(7) Bakowies, D.; Thiel, W. *J. Phys. Chem.* **1996**, *100*, 10580.

(8) Nasluzov, V. A.; Rivanenkov, V. V.; Gordienko, A. B.; Neyman, K. M.; Birkenheuer, U.; Rösch, N. *J. Chem. Phys.* **2001**, *115*, 8157.

(9) Nasluzov, V. A.; Rivanenkov, V. V.; Shor, A. M.; Neyman, K. M.; Birkenheuer, U.; N. Rösch, *Int. J. Quantum Chem.* **2002**, *90*, 386.

(10) (a) Gorb, L. G.; Rivail, J.-L.; Thery, V.; Rinaldi, D. *Int. J. Quantum Chem. Quantum Chem. Symp.* **1996**, *30*, 1525. (b) Zhang, Y.; Lee, T.-S.; Yang, W. *J. Chem. Phys.* **1999**, *110*, 46.

(11) Sulimov, V. B.; Sushko, P. V.; Edwards, A. H.; Shluger, A. L.; Stoneham, A. M. *Phys. Rev. B* **2002**, *66*, 024108.

(12) In embedding schemes utilizing formal charges in the MM part, strong polarization of oxygen centers in the border region is observed due to artificially large point charges assigned to neighboring classical cations. This problem is usually overcome by attaching pseudopotentials on these neighboring cations, as in our ionic EPE scheme.[8] In the present covEPE scheme, the charges of classical ions are compatible with the true electrostatic potential; as a result, no problems arise with an artificial polarization of O* centers.

(13) Catlow, C. R. A.; Mackrodt, W. C. In *Computer Simulations of Solids*; Catlow, C. R. A., Mackrodt, W. C., Eds.; Lecture Notes in Physics 166; Springer: Berlin, 1982; p 3.

(14) Breneman, C. M.; Wibery, K. B. *J. Comput. Chem.* **1990**, *11*, 361.

(15) ParaGauss 2.2, Belling, T.; Grauschopf, T.; Krüger, S.; Nörtemann, F.; Staufer, M.; Mayer, M.; Nasluzov, V. A.; Birkenheuer, U.; Hu, A.; Matveev, A. V.; Shor, A. M.; Fuchs-Rohr, M. S. K.; Neyman, K. M.; Ganyushin, D. I.; Kerdcharoen, T.; Woiterski, A.; Rösch, N. ParaGauss, version 2.2; Technische Universität München, 2001.

Covalent Oxides and Zeolites

J. Phys. Chem. B, Vol. 107, No. 10, 2003 **2241**

(16) Belling, T.; Grauschopf, T.; Krüger, S.; Mayer, M.; Nörtemann, F.; Staufer, M.; Zenger, C.; Rösch, N. In *High Performance Scientific and Engineering Computing*; Bungartz, H.-J., Durst, F., Zenger, C., Eds.; Lecture Notes in Computational Science and Engineering 8; Springer: Heidelberg, 1999; p 439.

(17) Dunlap, B. I.; Rösch, N. *Adv. Quantum Chem.* **1990**, *21*, 317.

(18) (a) Becke, A. D. *Phys. Rev. A* **1988**, *38*, 3098. (b) Perdew, J. P. *Phys. Rev. B* **1986**, *33*, 8822; **1986**, *34*, 7406.

(19) (a) Van Duijneveld, F. B. *IBM Res. Report RJ* **1971**, 945. (b) *Gaussian Basis Sets for Molecular Calculations*; Huzinaga, S., Ed.; Elsevier: Amsterdam, 1984. (c) Veillard, A. *Theor. Chim. Acta* **1968**, *12*, 405. (d) Bär, M. R.; Sauer, J. *Chem. Phys. Lett.* **1994**, *226*, 405.

(20) Chung, S. C.; Krüger, S.; Pacchioni, G.; Rösch, N. *J. Chem. Phys.* **1995**, *102*, 3695.

(21) Pople, J. A.; Gill, P. M. W.; Johnson, B. G. *Chem. Phys. Lett.* **1992**, *199*, 557.

(22) Gill, P. M. W.; Johnson, B. G.; Pople, J. A. *Chem. Phys. Lett.* **1993**, *209*, 506.

(23) Nasluzov, V. A.; Rösch, N. *Chem. Phys.* **1996**, *210*, 413.

(24) Gill, P. E.; Murray, W.; Wright, M. H.; In *Practical Optimization*; Academic Press: New York, 1981.

(25) Nasluzov, V. A.; Shor, A. M.; Nörtemann, F.; Staufer, M.; Yudanov, I. V.; Rösch, N. *J. Mol. Struct. THEOCHEM* **1999**, *466*, 235.

(26) Chirlian, L. E.; Francl, M. M. *J. Comput. Chem.* **1987**, *8*, 894. (b) Breneman, C. M. Wiberg, K. B. *J. Comput. Chem.* **1990**, *11*, 361.

(27) Frisch, M. J.; Trucks, G. W.; Schlegel, H. B.; Scuseria, G. E.; Robb, M. A.; Cheeseman, J. R.; Zakrzewski, V. G.; Montgomery, J. A., Jr.; Stratmann, R. E.; Burant, J. C.; Dapprich, S.; Millam, J. M.; Daniels, A. D.; Kudin, K. N.; Strain, M. C.; Farkas, O.; Tomasi, J.; Barone, V.; Cossi, M.; Cammi, R.; Mennucci, B.; Pomelli, C.; Adamo, C.; Clifford, S.; Ochterski, J.; Petersson, G. A.; Ayala, P. Y.; Cui, Q.; Morokuma, K.; Malick, D. K.; Rabuck, A. D.; Raghavachari, K.; Foresman, J. B.; Cioslowski, J.; Ortiz, J. V.; Stefanov, B. B.; Liu, G.; Liashenko, A.; Piskorz, P.; Komaromi, I.; Gomperts, R.; Martin, R. L.; Fox, D. J.; Keith, T.; Al-Laham, M. A.; Peng, C. Y.; Nanayakkara, A.; Gonzalez, C.; Challacombe, M.; Gill, P. M. W.; Johnson, B. G.; Chen, W.; Wong, M. W.; Andres, J. L.; Head-Gordon, M.; Replogle, E. S.; Pople, J. A. *Gaussian 98*, revision A.7; Gaussian, Inc.: Pittsburgh, PA, 1998.

(28) van Beest, B. W. H.; Kramer, G. J.; van Santen, R. A. *Phys. Rev. Lett.* **1991**, *64*, 1955.

(29) Jackson, R. A.; Catlow, C. R. A. *Mol. Simul.* **1988**, *1*, 207.

(30) Blake, N. P.; Weakliem P. C.; Metiu, H. *J. Phys. Chem.* **1998**, *102*, 67.

(31) Kramer, G. J.; Farragher, N. P.; van Beest, B. W. H.; van Santen, R. A. *Phys. Rev. B* **1991**, *43*, 5068.

(32) Nicholas, J. B.; Hopfinger, A. J.; Trouw, F. R.; Iton, L. E. *J. Am. Chem. Soc.* **1991**, *113*, 4792.

(33) (a) Gale, J. GULP, version 1.3, Imperial College, London. (b) Gale, J. D. *J. Chem. Soc., Faraday Trans.* **1997**, *93*, 629.

(34) Smith, L. J.; Davidson, A.; Cheetham, A. K. *Catal. Lett.* **1997**, *49*, 143.

(35) Wright, A. F.; Lehmann, M. S. J. *Solid State Chem.* **1981**, *36*, 371.

(36) McSkimin, H. J.; Andreat, P.; Thurston, R. N. *J. Appl. Phys.* **1965**, *36*, 1624.

(37) Dollare, W. A. *Z. Kristallogr.* **1965**, *121*, 369.

(38) (a) Díaz-Cabañas, M.-J.; Barrett, Ph. A.; Camblor, M. A. *Chem. Commun.* **1998**, 1882. (b) Baerlocher, Ch.; McCusker, L. B. Database of Zeolite Structures. http://www.iza-structure.org/databases/

(39) Feische, J.; Luger, S.; Baerlocher, Ch. *Zeolites* **1986**, *6*, 367.

(40) Parise, J. B.; Shannon, R. D.; Prince, E.; Cox, D. E. *Z. Kristallogr.* **1983**, *185*, 175.

(41) Stefanovich, E. V., Truong, T. N. *J. Phys. Chem. B* **1998**, *102*, 3018.

(42) Stevens, W. J.; Basch, H.; Krauss, M. *J. Chem. Phys.* **1984**, *81*, 6026.

(43) Jeanvoine, Y.; Angyan, J. G.; Kresse, G.; Hafner, J. *J. Phys. Chem. B* **1998**, *102*, 5573.

(44) van Santen, R. A.; Kramer, G. J. *Chem. Rev.* **1995**, *95*, 637.

(45) Ugliengo, P.; Civalleri, B.; Zicovich-Wilson, C. M.; Dovesi, R. *Chem. Phys. Lett.* **2000**, *318*, 247.

(46) Shah, R.; Gale, J. D.; Payne, M. C. *Phase Transitions* **1997**, *61*, 67.

(47) Shah, R.; Gale, J. D.; Payne, M. C. *J. Phys. Chem.* **1996**, *100*, 11688.

(48) Mihaleva, V. V.; van Santen, R. A.; Jansen, A. P. J. *J. Phys. Chem. B* **2001**, *105*, 6874.

(49) Strodel, P.; Neyman, K. M.; Knözinger, H.; Rösch, N. *Chem. Phys. Lett.* **1995**, *240*, 547.

(50) Vayssilov, G. N.; Rösch, N. *J. Phys. Chem. B* **2001**, *105*, 4277.

(51) Hriljac, J. A.; Eddy, M. M.; Cheetham, A. K.; Donohue, J. A.; Ray, G. J. *J. Solid State Chem.* **1993**, *106*, 66.